

## Anisotropic gradient driven domain wall motion in antiferromagnets

D. L. Wen<sup>1,\*</sup>, Z. Y. Chen<sup>1,\*</sup>, W. H. Li<sup>1</sup>, M. H. Qin<sup>1,†</sup>, D. Y. Chen<sup>1</sup>, Z. Fan<sup>1</sup>, M. Zeng<sup>1</sup>,  
X. B. Lu<sup>1</sup>, X. S. Gao<sup>1</sup>, and J. –M. Liu<sup>2</sup>

<sup>1</sup>*Institute for Advanced Materials, South China Academy of Advanced Optoelectronics and  
Guangdong Provincial Key Laboratory of Quantum Engineering and Quantum Materials,  
South China Normal University, Guangzhou 510006, China*

<sup>2</sup>*Laboratory of Solid State Microstructures and Innovative Center for Advanced  
Microstructures, Nanjing University, Nanjing 210093, China*

**[Abstract]** Searching for new energy-saving method of controlling antiferromagnetic (AFM) domain wall is one of the most important issues for AFM spintronic device design. In this work, we study theoretically and numerically the domain wall motion in AFM nanowires driven by electric voltage induced anisotropy gradient. The domain wall velocity depending on the gradient and intrinsic material properties are simulated based on the Landau-Lifshitz-Gilbert equation and also deduced using the energy dissipation theorem. The domain wall moves at a nearly constant velocity for small gradients, while accelerates for large gradients due to the enlargement of the domain wall width during the motion. Furthermore, the calculated results are confirmed to be independent of the lattice dimension. Comparing with those electric current driven methods, the anisotropy gradient driven domain wall motion through tuning electric voltage on particular heterostructures is expected to be more energy saving. Thus, our work unveils a promising method of controlling AFM domain walls, and does provide useful information for future AFM spintronic applications.

**Keywords:** antiferromagnetic dynamic, domain wall, magnetics anisotropic gradient

---

\*D Wen and Z Chen contributed equally to this work;

†E-mail: [qinmh@scnu.edu.cn](mailto:qinmh@scnu.edu.cn)

## I. Introduction

Nowadays, the interest in antiferromagnets significantly increases due to their potential applications for spintronics.<sup>1,2</sup> Comparing with ferromagnets based storage devices, antiferromagnets based devices are more stable against perturbing magnetic fields and could be designed with high element densities without producing any stray fields, attributing to zero net magnetization and ultralow susceptibility in antiferromagnetic (AFM) elements.<sup>3-5</sup> Moreover, AFM materials show fast magnetic dynamics including the spin wave modes with high frequencies resulted from their complex spin configurations, which favors them for promising potentials in future devices.<sup>6</sup>

One of the major challenges for AFM spintronic applications is how to manipulate AFM domain walls (DWs), and a number of driving methods including spin waves,<sup>7</sup> spin-orbit torques,<sup>8,9</sup> asymmetric magnetic fields,<sup>10</sup> and thermal gradients<sup>11-13</sup> have been theoretically proposed to drive DWs in antiferromagnets. For example, a high speed  $\sim 30$  km/s of the DW motion was predicted driven by the electrical current induced Néel spin-orbit torques which are available in CuMnAs<sup>14</sup> and Mn<sub>2</sub>Au<sup>15</sup>. Furthermore, it has been revealed that the competition between the entropic torque and the Brownian force under temperature gradient determines the direction of the DW motion. Importantly, in these control schemes, the AFM DWs remain non-tilted, and the high wall mobility is suggested due to the absence of the walker breakdown<sup>16,17</sup> which limits the motion of typical ferromagnetic DWs.

These proposed methods are very meaningful for future experiments and device design, while several shortcomings still deserve to be overcome. For example, the Néel spin-orbit torques only arise in particular antiferromagnets with locally broken inversion symmetry and drives the neighboring DWs approach to each other and annihilates them, strongly hindering their applications. Furthermore, other methods such as temperature gradient and spin wave driven DWs motions seem to be schemes with more theoretical sense rather than realistic sense, which are hard to be realized in experiments. Thus, finding new energy-saving methods of controlling the AFM DWs is still of great importance for future applications.

Fortunately, the voltage-controlled magnetic anisotropies have been experimentally revealed in magnetic heterostructures,<sup>18-22</sup> and anisotropy gradients can be obtained through elaborately structure design. Interestingly, under such a gradient, the AFM domain wall (DW)

tends to move towards the low anisotropy side to save the system energy. More importantly, comparing with the electrical current driven schemes generating considerable Joule heat, the voltage driven scheme is certainly more energy-saving and also works for insulators. As a matter of fact, the anisotropy gradient has been proven to efficiently drive the skyrmions motion,<sup>23-25</sup> which could be also utilized to control the AFM DWs. However, AFM DW dynamics under anisotropy gradient has not been reported, as far we know. Thus, this subject urgently deserves to be investigated numerically and theoretically in order to promote the application process for AFM spintronics, noting that the current technical limitation of experiments hinders a systematically study of AFM DW motion.

In this work, we study the anisotropy gradient driven AFM DW motion in AFM nanowires. The velocity depending on the gradient and intrinsic physical parameters are simulated based on the Landau-Lifshitz-Gilbert (LLG) equation and also deduced by the energy dissipation theorem. It is observed that the DW moves at a nearly constant velocity for small gradients, while accelerates for large gradients due to the enlargement of the domain wall width during the motion. Moreover, the calculated results are confirmed to be independent of the lattice dimension.

## II. Model and method

We study an one-dimensional AFM model with isotropic Heisenberg exchanges between the nearest neighbors and a uniaxial anisotropy term<sup>26</sup>

$$H = J \sum_{\langle i,j \rangle} \mathbf{S}_i \cdot \mathbf{S}_j - \sum_i d_i^z (S_i^z)^2, \quad (1)$$

where  $J > 0$  is the AFM coupling constant,  $\mathbf{S}_i = \boldsymbol{\mu}_i / \mu_s$  represent the normalized magnetic moment at site  $i$  with the three components  $S_i^x$ ,  $S_i^y$  and  $S_i^z$ . The second term is the anisotropy energy with the easy axis in the  $z$  direction, and the anisotropy gradient is introduced by  $d_i^z = d_0 + i \cdot \Delta d$  where  $\Delta d$  describes the gradient magnitude. The AFM dynamics is investigated by solving the LLG equation based on the atomistic spin model,<sup>27,28</sup>

$$\frac{\partial \mathbf{S}_i}{\partial t} = -\frac{\gamma}{\mu_s(1+\alpha)^2} \mathbf{S}_i \times [\mathbf{H}_i + \alpha(\mathbf{S}_i \times \mathbf{H}_i)], \quad (2)$$

where  $\gamma = 1$  is the gyromagnetic ratio,  $\alpha = 0.002$  is the Gilbert damping constant,  $\mathbf{H}_i =$

$-\partial H/\partial \mathbf{S}_i$  is the effective field. Unless stated elsewhere, the LLG simulations are performed on the lattice (lattice parameter  $a$ ) with  $1 \times 1 \times 400$  spins with open boundary conditions using fourth-order Runge-Kutta method with a time step  $\Delta t = 1.0 \times 10^{-4} \mu_s/\gamma J$ . The local staggered magnetization  $2\mathbf{n} = \mathbf{m}_1 - \mathbf{m}_2$  is calculated to describe the spin dynamics where  $\mathbf{m}_1$  and  $\mathbf{m}_2$  are the magnetizations of the two sublattices. After sufficient relaxation of the DW, the anisotropy gradient is applied to drive the DW motion, as depicted in Fig. 1.

### III. Simulation results and discussion

Fig. 2(a) presents the profiles of the DW at different times ( $t$ ) for  $d_0 = 0.01J$  and  $\Delta d = 6 \times 10^{-6}J/a$ , which clearly demonstrates the motion of the DW under the anisotropy gradient. After a quick acceleration, the DW moves towards the lower anisotropy region with a nearly constant velocity. Moreover, the DW is rather robust and remains in its initial plane during the motion. The simulated DW position and energy as functions of time are shown in Fig. 2(b) which clearly demonstrates the decrease of the energy with the motion of the DW. Furthermore, the trajectory of  $\mathbf{n}$  depends not only on its instantaneous position but also on the velocity.<sup>29</sup> Thus,  $\mathbf{n}$  tends to continue its path even after reaching the equilibrium position (along its effective field), resulting in the weak fluctuation of the DW energy.

As a matter of fact, the motion of the DW can be qualitatively understood from the competition between various torques acting on the DW, as depicted in Fig. 2(c). In the absence of the anisotropy gradient, the DW structure is symmetric with respect to its central plane. The symmetry is broken by the consideration of the gradient. Specifically, for the two neighbors ( $\mathbf{S}_L$  and  $\mathbf{S}_R$ ) of the DW central spin  $\mathbf{S}_0$ , the damping torque resulted from the anisotropy term on  $\mathbf{S}_L$  is smaller than that on  $\mathbf{S}_R$ , leading to the fact that  $\mathbf{S}_L$  deviates from the easy axis stronger. As a result, the damping torque on  $\mathbf{S}_0$  from the exchange interaction with  $\mathbf{S}_R$   $\Gamma_R^d$  is larger than that with  $\mathbf{S}_L$   $\Gamma_L^d$ , resulting in the net damping torque  $\sim (\Gamma_R^d + \Gamma_L^d)$  which efficiently drive the DW motion to the low anisotropy region. Undoubtedly, the net driven torque increases with the increase of gradient, which significantly enhances the DW motion, as clearly shown in Fig. 2(d) which presents the simulated DW position as a function of time for various  $\Delta d$ .

In order to uncover the physics more clearly, we calculate the velocity of the DW motion from the perspective of the energy conservation. First, considering that the DW motion originates from the dissipation of the DW energy  $E_{DW} = 2(2Jd_c)^{1/2}$  with  $d_c$  is the anisotropy constant on  $S_0$ ,<sup>30</sup> the Rayleigh dissipation function  $R = \alpha\rho|\dot{\mathbf{n}}|^2 dz/2$  is introduced to describe the energy dissipation of the system,<sup>31</sup> where  $\rho = \mu_s/\gamma a$  is the density of the staggered spin angular momentum per unit cell, and  $\dot{\mathbf{n}}$  represents the derivative with respect to time. Subsequently, according to the classical mechanics, we obtain

$$\frac{dE_{DW}}{dt} = -2R. \quad (3)$$

After performing necessary substitutions and simplifications, we obtain the velocity of DW motion under the anisotropy gradient,

$$v = \frac{\gamma\lambda^2\Delta d}{\alpha\mu_s}, \quad (4)$$

where  $\lambda = a(J/2d_c)^{1/2}$  is the width of the DW.

It is indicated in Eq. (4) that the velocity of the DW also depends on  $d_c$  or  $d_0$ , which has been confirmed in our simulations. Fig. 3(a) gives the simulated DW position as a function of  $t$  for various  $d_0$  for  $\Delta d = 4 \times 10^{-6} J/a$ . With the enhancement of the anisotropy, the DW motion is significantly suppressed. In Fig. 3(b), the simulated (empty dots) and calculated (solid lines) velocities as functions of  $\Delta d$  for various  $d_0$  are presented, which clearly shows that the simulations and calculations well coincide with each other especially for small  $\Delta d$ .

The effect of the damping constant  $\alpha$  on the DW velocity is also investigated, and the corresponding results are shown in Fig. 3(c) which gives the simulated and calculated velocities as functions of  $\alpha$  for various  $\Delta d$  for  $d_0 = 0.01J$ . It is noted that an enhanced damping term always lowers the mobility of the DW, and the velocity decreases with the increase of  $\alpha$ . Furthermore, the DW width is simply considered to be a constant during the motion of the DW, which well describes the case of small  $\Delta d$ . However, for large  $\Delta d$ , the DW width is expected to increase with the motion of the DW toward the low anisotropy side, resulting in the additional acceleration of the DW motion. In order to better understand the acceleration behavior, we investigated the DW motion under huge anisotropy gradient  $\Delta d = 0.0003J/a$ . The simulated DW position and velocity are presented in Fig. 3(d), which clearly shows that the

velocity linearly increases with  $t$ .

So far, the anisotropy gradient driven DW motion has been studied based on the one-dimensional model. However, the results and conclusions also apply to AFM films and bulks, as shown in Fig. 4(a) which presents the simulated DW velocity as a function of  $\Delta d$  for various lattice dimensions for  $d_0 = 0.01J$  and  $\alpha = 0.002$ . All the curves are well consistent with each other especially under small  $\Delta d$ , indicating that the DW velocity hardly depends on the lattice dimension. This phenomenon can be qualitatively understood from the energy landscape. For a small  $\Delta d$  under which a rather robust DW is available, the spin configuration of the DW is almost the same as the static one. In this case, for every cross-section perpendicular to  $z$  axis, the neighboring spins still align antiparallel to each other, and the exchange energy is satisfied. Thus, the energy difference between neighboring unit cross sections only arises from the single-ion anisotropy term and remains unchanged for various dimensions, resulting in the invariant force density exerted on the DW. As a result, the DW dynamics is hardly affected by the lattice dimension. Specifically, for  $\Delta d/d_c = 1 \times 10^{-4} a^{-1}$  and  $\alpha = 0.002$ , the velocity of the DW for NiO with the exchange stiffness  $A \approx 5 \times 10^{-13} \text{ J/m}$ ,  $a \approx 4.2 \text{ \AA}$ ,  $\mu_s \approx 1.7 \mu_B$  where  $\mu_B$  is the Bohr magneton is estimated to be  $\sim 100 \text{ m/s}$ .

At last, we check the dependence of the DW dynamics on Dzyaloshinskii-Moriya interaction (DMI) which may be available in some realistic materials.<sup>32,33</sup> Here, the DMI energy  $\Sigma_i \mathbf{D}_i \cdot (\mathbf{S}_i \times \mathbf{S}_{i+1})$  with  $\mathbf{D}_i = D(0, 0, 1)$  is considered, and the simulated results based on the LLG dynamics are presented in Fig. 4(b), where the  $v(D)$  curves upon various  $\Delta d$  are plotted. For a fixed  $\Delta d$ ,  $v$  gradually increases with the increase of  $D$ , indicating that the DMI enhances the DW motion, similar to the earlier reports.<sup>34,35</sup> When the DMI is considered, the DW energy decreases to  $E_{DW} = 2(2Jd_c - D^2)^{1/2}$ ,<sup>36,37</sup> resulting in the increases of the DW width and velocity for a fixed  $\Delta d$ . In detail, the DW width is increased to<sup>38</sup>

$$\lambda = \lambda_0 \left( 1 - \frac{D^2}{2Jd_c} \right)^{-\frac{1}{2}}, \quad (5)$$

with  $\lambda_0 = a(J/2d_c)^{1/2}$ . Then, the velocity can be expressed as

$$v = \frac{\gamma \Delta d \lambda^2}{\alpha \mu_s}, \quad (6)$$

In Fig. 4(b), the calculated curves from Eq. (6) are also plotted, which are well consistent

with the simulated curves.

#### **IV. Conclusion**

In summary, we have studied the AFM DW motion under anisotropy gradient based on the one-dimensional model. The DW velocity depending on the gradient magnitude and intrinsic physical parameters are simulated based on the LLG equation and also derived theoretically based on the energy dissipation theorem. The DW is rather robust for small gradients and moves at a nearly constant velocity, while accelerates for large gradients due to the enlargement of the DW width during its motion. Moreover, the calculated results are confirmed to be independent of the lattice dimension. Interestingly, anisotropy gradient could be easily obtained through tuning electric voltage on particular heterostructures, and the modulation is expected to be more energy saving and with less Joule heat, comparing with those electric current driven methods. Thus, our work unveils a promising method of controlling AFM DWs, and does provide useful information for future spintronic applications.

#### **Acknowledgment**

The work is supported by the National Key Projects for Basic Research of China (Grant No. 2015CB921202), and the Natural Science Foundation of China (No. 11204091), and the Science and Technology Planning Project of Guangdong Province (Grant No. 2015B090927006), and the Natural Science Foundation of Guangdong Province (Grant No. 2016A030308019).

## ***References:***

1. R. Cheng, J. Xiao, Q. Niu, and A. Brataas, Phys. Rev. Lett. **113**, 057601 (2014).
2. E. Gomonay and V. Loktev, Low. Temp. Phys+. **40**, 17 (2014).
3. V. Baltz, A. Manchon, M. Tsoi, T. Moriyama, T. Ono, and Y. Tserkovnyak, Rev. Mod. Phys. **90**, 015005 (2018).
4. O. Gomonay, T. Jungwirth, and J. Sinova, Phys. Status Solidi RRL **11**, 1770319 (2017).
5. Marrows and Christopher, Science **351**, 558 (2016).
6. T. Kampfrath *et al.*, Nat. Photonics **5**, 31 (2011).
7. W. Yu, J. Lan, and J. Xiao, Phys. Rev. B **98**, 144422 (2018).
8. O. Gomonay, T. Jungwirth, and J. Sinova, Phys. Rev. Lett. **117**, 017202 (2016).
9. P. Wadley *et al.*, Science **351**, 587 (2016).
10. Y. L. Zhang, Z. Y. Chen, Z. R. Yan, D. Y. Chen, Z. Fan, and M. H. Qin, Appl. Phys. Lett. **113**, 112403 (2018).
11. S. K. Kim, O. Tchernyshyov, and Y. Tserkovnyak, Phys. Rev. B **92**, 020402 (2015).
12. S. Selzer, U. Atxitia, U. Ritzmann, D. Hinzke, and U. Nowak, Phys. Rev. Lett. **117**, 107201 (2016).
13. Z. R. Yan, Z. Y. Chen, M. H. Qin, X. B. Lu, X. S. Gao, and J. M. Liu, Phys. Rev. B **97**, 054308 (2018).
14. K. Olejník *et al.*, Sci. Adv. **4**, eaar3566 (2018).
15. S. Y. Bodnar *et al.*, Nat. Commun. **9**, 348 (2018).
16. X. R. Wang, P. Yan, J. Lu, and C. He, Ann. Phys-new. York. **324**, 1815 (2009).
17. A. Mougin, M. Cormier, J. P. Adam, P. J. Metaxas, and J. Ferré Europhys. Lett. **78**, 57007 (2007).
18. T. Nozaki, T. Yamamoto, S. Tamaru, H. Kubota, A. Fukushima, Y. Suzuki, and S. Yuasa, APL Mater. **6**, 026101 (2018).
19. S. Z. Peng *et al.*, Appl. Phys. Lett. **111**, 152403 (2017).
20. X. Li *et al.*, Appl. Phys. Lett. **110**, 052401 (2017).
21. Z. Wen, H. Sukegawa, T. Seki, T. Kubota, K. Takanashi, and S. Mitani, Sci. Rep. **7**, 45026 (2017).



22. A. K. Shukla, M. Goto, X. Xu, K. Nawaoka, J. Suwardy, T. Ohkubo, K. Hono, S. Miwa, and Y. Suzuki, *Sci. Rep.* **8**, 10362 (2018).
23. X. Wang, W. Gan, J. Martinez, F. Tan, M. Jalil, and W. Lew, *Nanoscale* **10**, 733 (2018).
24. H. Y. Xia, C. K. Song, C. D. Jin, J. S. Wang, J. B. Wang, and Q. F. Liu, *J. Magn. Magn. Mater.* **458**, 57 (2018).
25. L. C. Shen, J. Xia, G. P. Zhao, X. C. Zhang, M. Ezawa, O. A. Tretiakov, X. X. Liu, and Y. Zhou, *Phys. Rev. B* **98**, 134448 (2018).
26. F. D. M. Haldane, *Phys. Rev. Lett.* **50**, 1153 (1983).
27. D. Hinzke and U. Nowak, *Phys. Rev. Lett.* **107**, 027205 (2011).
28. P. Yan, X. S. Wang, and X. R. Wang, *Phys. Rev. Lett.* **107**, 177207 (2011).
29. Y. G. Semenov, X.-L. Li, and K. W. Kim, *Phys. Rev. B* **95**, 014434 (2017).
30. K. M. Pan, L. D. Xing, H. Y. Yuan, and W. W. Wang, *Phys. Rev. B* **97**, 184418 (2018).
31. S. K. Kim, Y. Tserkovnyak, and O. Tchernyshyov, *Phys. Rev. B* **90**, 104406 (2014).
32. K.-S. Ryu, L. Thomas, S.-H. Yang, and S. Parkin, *Nat. Nanotechnol.* **8**, 527 (2013).
33. S. Emori, U. Bauer, S.-M. Ahn, E. Martinez, and G. S. Beach, *Nat. Mater.* **12**, 611 (2013).
34. S. G. Je, D. H. Kim, S. C. Yoo, B. C. Min, K. J. Lee, and S. B. Choe, *Phys. Rev. B* **88**, 214401 (2013).
35. D. H. Kim, D. Y. Kim, S. C. Yoo, B. C. Min, and S. B. Choe, *Phys. Rev. B* **99**, 134401 (2019).
36. W. C. Yu, J. Lan, and J. Xiao, *Phys. Rev. B* **98**, 144422 (2018).
37. A. Qaiumzadeh, L. A. Kristiansen, and A. Brataas, *Phys. Rev. B* **97**, 020402 (2018).
38. Y. Yamane, *Phys. Rev. B* **98**, 174434 (2018).

## FIGURE CAPTIONS

FIG. 1. (color online) Illustration of a domain wall in antiferromagnetic nanowire in an anisotropy gradient.

FIG. 2. (color online) (a) Profile of the DW at different times in the antiferromagnetic nanowire, and (b) the position and DW energy of the DW as functions of time for  $\Delta d = 6 \times 10^{-6} J/a$  and  $d_0 = 0.01 J$ . (c) A schematic depiction of torques acting on DW spins under an anisotropic gradient, and (d) the position of the DW versus time for various  $\Delta d$  for  $d_0 = 0.01 J$ .

FIG. 3. (color online) (a) The position of the DW as a function of time for various  $d_0$  for  $\Delta d = 4 \times 10^{-6} J/a$ . The simulated (empty points) and calculated (solid lines) velocities as functions of (b)  $\Delta d$  for various  $d_0$  for  $\alpha = 0.002$ , and (c)  $\alpha$  for various  $\Delta d$  for  $d_0 = 0.01 J$ . (d) The simulated DW position and velocity as functions of time for large  $\Delta d = 0.0003 J/a$ .

FIG. 4. (color online) (a) The simulated DW velocity as a function of  $\Delta d$  for various lattice sizes, and (b) The simulated (empty points) and calculated (solid lines) velocities as functions of  $D$  for various  $\Delta d$ .

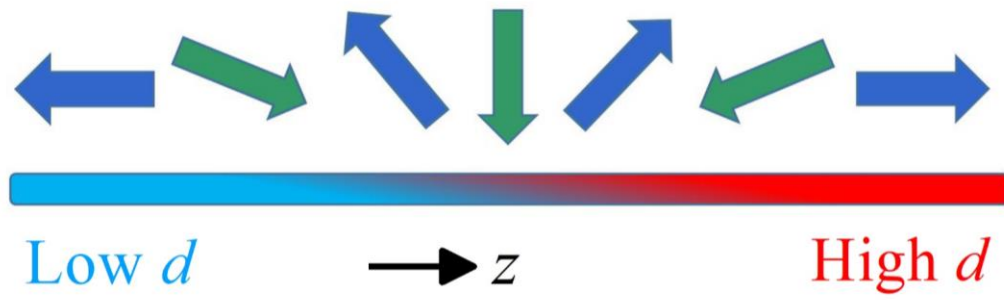


FIG. 1. (color online) Illustration of a domain wall in antiferromagnetic nanowire in an anisotropy gradient.

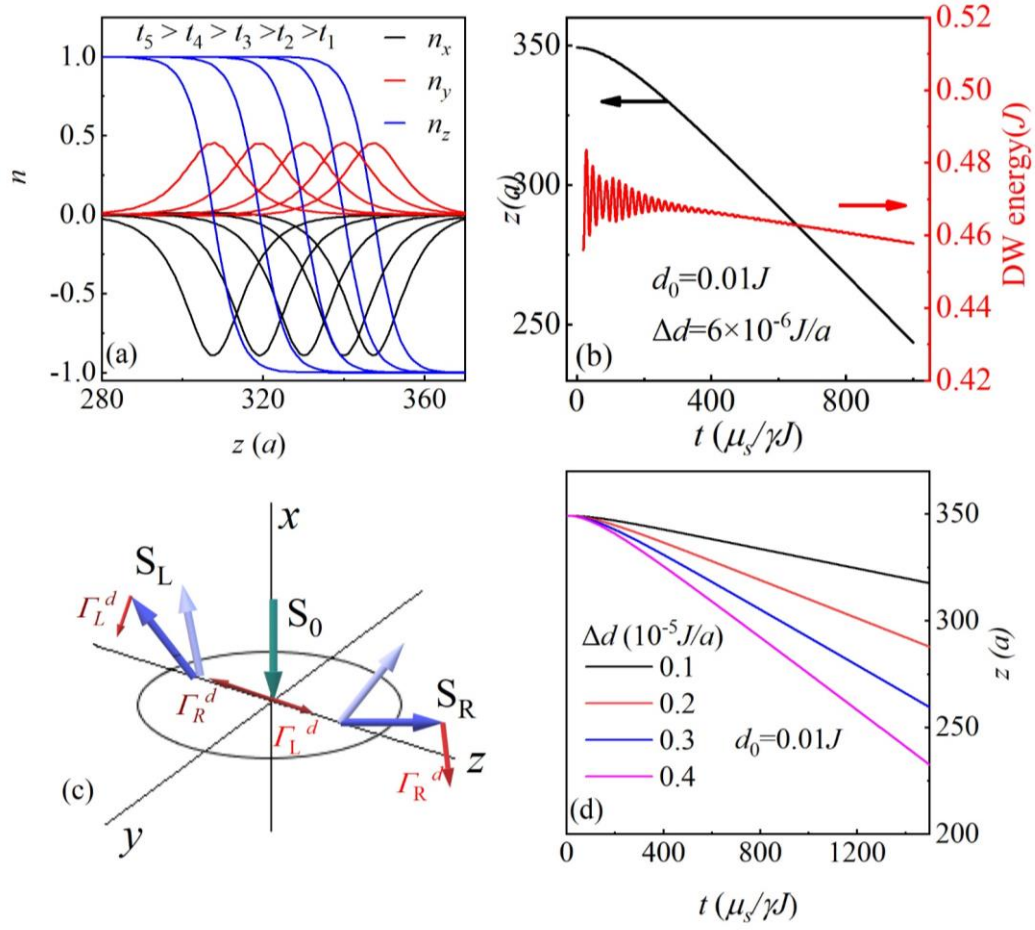


FIG. 2. (color online) (a) Profile of the DW at different times in the antiferromagnetic nanowire, and (b) the position and DW energy of the DW as functions of time for  $\Delta d = 6 \times 10^{-6} J/a$  and  $d_0 = 0.01 J$ . (c) A schematic depiction of torques acting on DW spins under an anisotropic gradient, and (d) the position of the DW versus time for various  $\Delta d$  for  $d_0 = 0.01 J$ .

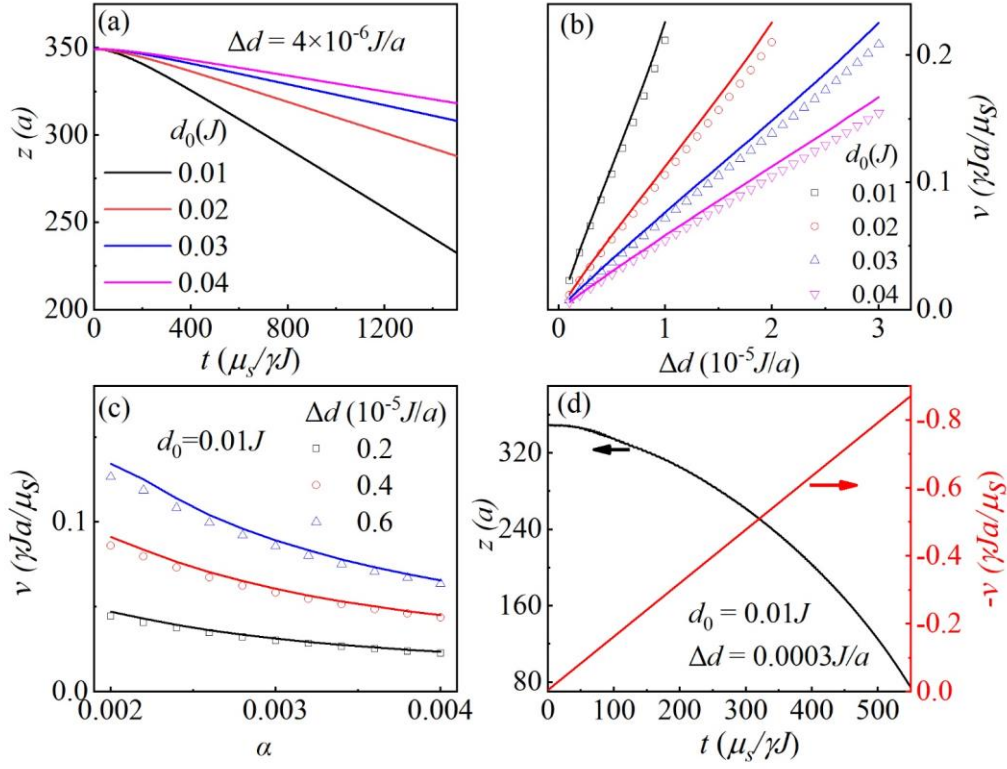


FIG. 3. (color online) (a) The position of the DW as a function of time for various  $d_0$  for  $\Delta d = 4 \times 10^{-6} J/a$ . The simulated (empty points) and calculated (solid lines) velocities as functions of (b)  $\Delta d$  for various  $d_0$  for  $\alpha = 0.002$ , and (c)  $\alpha$  for various  $\Delta d$  for  $d_0 = 0.01 J$ . (d) The simulated DW position and velocity as functions of time for large  $\Delta d = 0.0003 J/a$ .

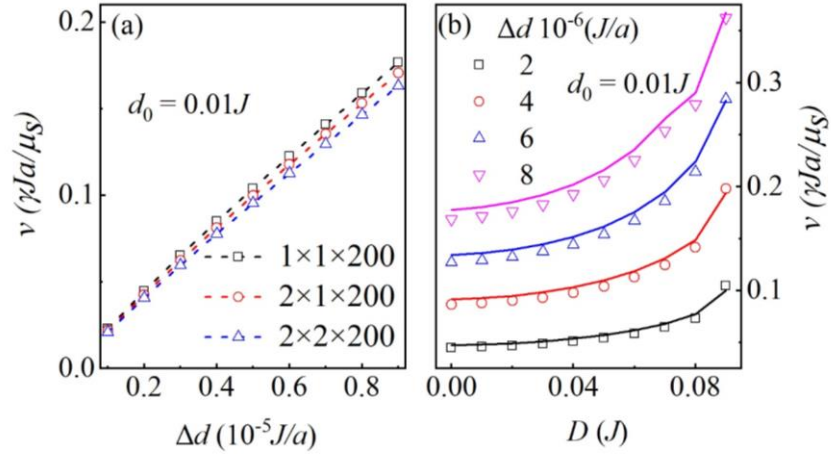


FIG. 4. (color online) (a) The simulated DW velocity as a function of  $\Delta d$  for various lattice sizes, and (b) The simulated (empty points) and calculated (solid lines) velocities as functions of  $D$  for various  $\Delta d$ .